Suppression of grain growth by additive in nanostructured p-type bismuth antimony tellurides

Citation: Zhang, Qian, Qinyong Zhang, Shuo Chen, Weishu Liu, Kevin Lukas, Xiao Yan, Hengzhi Wang, et al. "Suppression of Grain Growth by Additive in Nanostructured p-Type Bismuth Antimony Tellurides." Nano Energy 1, no. 1 (January 2012): 183–189.

As Published: http://dx.doi.org/10.1016/j.nanoen.2011.10.006

Publisher: Elsevier

Persistent URL: http://hdl.handle.net/1721.1/103945

Version: Author's final manuscript: final author's manuscript post peer review, without publisher's formatting or copy editing

Suppression of grain growth by an additive in nanostructured p-type bismuth antimony tellurides

Qian Zhang[a], Qinyong Zhang[a], Shuo Chen[a], Weishu Liu[a], Kevin Lukas[a], Xiao Yan[a], Hengzhi Wang[a], Dezhi Wang[a], Cyril Opeil[a], Gang Chen[b,*], and Zhifeng Ren[a,**]

[a]*Department of Physics, Boston College, Chestnut Hill, Massachusetts 02467*

[b]*Department of Mechanical Engineering, Massachusetts Institute of Technology, Cambridge, Massachusetts 02139*

Abstract

Grain growth during hot pressing is a major issue in the preparation of nanostructured bismuth-antimony-tellurides during hot-pressing the nanopowders into dense bulk samples. To prevent grain agglomeration during ball milling and growth during hot pressing, organic agent (Oleic Acid, OA) as additive was added into the materials at the beginning of the ball milling process. With different concentrations of OA (0.5, 1.0, 1.5, 2.0, and 2.5 wt.%), grains with different sizes are obtained. Structural analysis clearly shows that it is the particle size of the nanopowders that determines the final grain size in the densely compacted bulk samples. A combination of small grains ~200-500 nm and nanopores leads to effective phonon scattering, which results in the decrease of lattice thermal conductivity, and ZT to ~1.3 at 373 K for the sample with a 2.0 wt.% OA as agent.

Key words: thermoelectrics, bismuth antimony tellurides, nanostructure, ball milling, hot pressing, surface energy

*Corresponding author. Tel: +1 617-253-0006, Fax: +1 617-324-5519, E-mail: gchen2@mit.edu

Address: Department of Mechanical Engineering, Massachusetts Institute of Technology, Cambridge, Massachusetts 02139, USA

**Corresponding author. Tel: +1 617-552-2832, Fax: +1 617-552-8478, E-mail: renzh@bc.edu

Address: Department of Physics, Boston College, Chestnut Hill, Massachusetts 02467, USA

1. Introduction

Thermoelectric (TE) devices that convert energy between heat and electricity have been a focused research field recently [1-3]. The energy conversion efficiency increases with a dimensionless thermoelectric figure-of-merit (*ZT*), defined as $(S^2\sigma/\kappa)T$, where *Z* is the figure-of-merit, *T* the absolute temperature, *S* the Seebeck coefficient, σ the electrical conductivity, and κ the total thermal conductivity with contributions from the lattice (κ_L) and the charge carriers (κ_e). The materials with high electrical conductivity, high Seebeck coefficient and low thermal conductivity are needed to achieve good *ZT* values. Bi_2Te_3-based materials are the best TE materials commercially used around room temperature (200-400 K). Great efforts have been devoted to improve this class of materials [4-7]. Recent research shows that nanostructures produced in p-type Bi_2Te_3-based bulk materials can significantly enhance the *ZT* value by reducing the thermal conductivity via effective phonon scattering without too much affecting the power factor ($S^2\sigma$) [8, 9]. Bulk materials with different nanostructures embedded in the $Bi_xSb_{2-x}Te_3$ matrix are achieved by hot pressing nanopowders prepared by various methods, such as hydrothermal technique [4, 11], ball milling [10], and melt spinning [12]. Hetero nanopowders such as fullerene, nano-SiC, nano-ZnAlO, etc., are also embedded in the $Bi_xSb_{2-x}Te_3$ matrix to act as phonon scattering centers to enhance *ZT* [13-15].

To effectively scatter phonons, it is desired to preserve nanostructures in bulk materials. Usually, the spark plasma sintering (SPS) technique is employed with a relatively short sintering time, which can suppress the grain growth to some extent [12, 16, 19]. However, in spite of the controllable particle size that has been obtained in the starting nanopowders, the grain growth during the sintering process is still a big issue [16-18], where the grains easily grow to micron-size, which degrades the nano-effect. For example, by ball milling the commercial ingots or elemental chunks and following with hot pressing, *ZT* values of ~1.4 or ~1.3 at about 373 K have been achieved, respectively [4, 11]. Nanograins in the bulk materials are considered beneficial to decreasing the thermal conductivity. However, there are still substantial amount of grains larger than 1 μm [17]. We postulate that the large surface energy possessed by the ultrafine ball milled nanopowders results in grain

aggregation to form much larger particles, and that it is these large particles to form the final grain size during the hot pressing causing grain growth. In the present work, small amount of well-chosen surfactant as additive is added into the samples while ball milling to lower the surface energy and get uniform smaller grains after hot pressing, leading to the decreased lattice thermal conductivity and subsequently a peak ZT ~1.3 at 373 K. It is worth to point out that such ZT values is about the best we have achieved before without the additives because of a degraded power factor when additive is used in the current study.

2. Experimental Procedure

Stoichiometric Bi (99.999%), Sb (99.999%), and Te (99.999%) were weighted and melted to form ingot $Bi_{0.4}Sb_{1.6}Te_3$. With different concentrations of the additive agent (Oleic Acid, OA, 99%, Alfa Aesar) (x = 0, 0.5, 1.0, 1.5, 2.0, and 2.5 wt.% per chemical formula weight), the ingots of $Bi_{0.4}Sb_{1.6}Te_3/x$ were ball milled for 4 hours. The ball milled powders were then loaded into a graphite die with an inner diameter of 12.7 mm and hot-pressed by direct current (dc-HP) press, first at 360 ^{o}C for 2 minutes to evaporate the OA, then at 450 ^{o}C for 2 minutes to produce the final discs for the measurements. X-ray diffraction analysis was conducted on a PANalytical multipurpose diffractometer with an X'celerator detector (PANalytical X'Pert Pro). The microstructures were investigated by a scanning electron microscope (SEM, JEOL 6340F) and a high resolution transmission electron microscope (HRTEM, JEOL 2010F). For HRTEM observations of the as-prepared powders, the samples were dispersed ultrasonically in ethanol for 5 minutes. A few droplets of the dispersion was placed on holy carbon coated copper grids and dried in air. The electrical resistivity (ρ) and the Seebeck coefficient were simultaneously measured on a commercial system (ULVAC ZEM-3) using the four-point dc current-switching method and the static temperature difference method. The thermal diffusivity (α) and the specific heat (C_p) were measured on a laser flash apparatus (Netzsch LFA 447) and a thermal analyzer (Netzsch DSC200-F3), respectively. The volumetric density (D) was quantified by an Archimedes method and listed in Table 1. The thermal conductivity κ was calculated from the relationship $\kappa = D\alpha C_p$. The Hall Coefficient R_H was measured using the PPMS (Physical Properties Measurement System,

Quantum Design) at room temperature. The carrier concentration n and Hall mobility μ_H were calculated using the relations $n = 1/eR_H$ and $\mu_H = \sigma R_H$, respectively.

3. Results and Discussions

XRD shows that single phase is obtained for all ingots by melting. The $Bi_{0.4}Sb_{1.6}Te_3$ ingots were then ball milled with different concentrations of additive OA and followed with hot pressing. Figure 1 shows the XRD patterns of the as-prepared disc samples. There is no difference of peak positions in all the samples. All the peaks can be indexed to the hexagonal structure (space group R3m). The SEM, TEM, and HRTEM images of the ball milled nanopowders without OA are shown in Fig. 2 (a)-(c). Although ball milling can decrease individual grains efficiently down to ~10 nm (Fig. 2(c)), which is consistent with the previous reports [4, 11], the surface energy increases correspondingly and makes it easy to form lots of micron-size aggregated particles, as shown in Fig. 2(a) and (b). It is very likely that after hot pressing, the majority of the aggregated particles grow to micron size grains, as presented in Fig. 3(a).

In order to reduce the surface energy, several kinds of ball milling agents as additive are tried. The best results so far are from samples with a 2 wt.% Oleic Acid (OA). Figure 2 (d)-(e) are the SEM, TEM and HRTEM images of the ball milled nanopowder with 2 wt.% OA, respectively. We noticed that even with the lubrication from OA coating during ball milling, which may reduce the energy transfer from the balls to the ingots, the ball milling is still powerful enough to break the ingots to ~10 nm fine grains. With OA, the particle size before hot-pressing is obviously smaller because of the less agglomeration, which is shown in Fig. 2(d) and (e). Correspondingly, the grain size in the final disc samples is decreased obviously after hot-pressing. The SEM images from the freshly fractured surface of the bulk samples with different concentrations of OA are shown in Fig. 3(b)-(f). With increasing concentration of OA, the grain size decreases to ~ 200-500 nm. The grain size is uniform when x is more than 2.0 wt.%. Furthermore, the additive begins to evaporate when the temperature is higher than the boiling point of OA (360 ^oC) during sintering, leaving lots of nanopores inside the samples, which is reflected in the reduced relative densities to

~90%-95% of the theoretical density.

We measured the TE properties parallel and perpendicular to the press directions. The nonflake structure and the random distribution create no anisotropy in all the samples. The temperature dependences of the electrical conductivity and Seebeck coefficient of the as-prepared $Bi_{0.4}Sb_{1.6}Te_3/x$ with x = 0, 0.5, 1.0, 1.5, 2.0, and 2.5 wt.% are presented in Fig. 4(a) and (b). The electrical conductivity is decreased with the increase of OA, likely due to the small amount of the organic agent left as well as the nanopores created when OA evaporates. The Hall measurements in table 1 show the results of the carrier concentration (n) and the mobility (μ) at room temperature, which affect the electrical conductivity (σ) by the relationship $\sigma = ne\mu$. The decrease in the electrical conductivity is obviously connected with the decrease in the carrier concentration. We consider that the coated OA during the ball milling process depresses the creation of defects, such as the Te vacancy and the Sb_{Te} anti-site deficiency, which decreases the concentration of the holes. However, the mobility is maintained in spite of the increased grain boundaries and the dispersed nanoholes, which are beneficial for the decrease of the thermal conductivity.

Figure 4 (e) and (f) present the total thermal conductivity and the lattice thermal conductivity of the samples ball milled with different concentrations of OA, respectively. The total thermal conductivity κ is the sum of the carrier thermal conductivity κ_e and the lattice thermal conductivity κ_L. We estimate κ_e from the Wiedemann-Franz relation, $\kappa_e = L\sigma T$, with the Lorenz number L taken as 1.6×10^{-8} V^2K^{-2} based on a previous calculation [20]. Although ball milling produces nanograins and interfaces that reduce lattice thermal conductivity [4, 11], there are still larger-sized grains caused by non-uniform ball milling, agglomeration and the grain growth during the hot-pressing. With an increase of OA, the grain size is decreased and becomes more uniform. Both the decreased grain size and the nanopores created in the sample preparation scatter phonons, leading to a large reduction in the lattice thermal conductivity. With a 2.5 wt.% OA, the lattice thermal conductivity decreases about 30%. The highest ZT value reaches 1.3 at about 373 K for samples with x = 2.0 and 2.5 wt.% (Fig. 4(f)). We also present the temperature dependence of the thermal diffusivity and specific heat of all the samples in Fig. 4(g) and (h), respectively. The increase on the specific heat is likely due to the remaining carbon. The organic residue and the relative low density may also deteriorate

the electrical properties, which may be solved by purifying the powder before hot-pressing.

Even though we decreased the grain size by using additives during balling milling for having achieved lower thermal conductivity, we did not achieve too much improvement in *ZT* values due to the fact that the additives have also decreased the power factor. Nevertheless, the grain size suppression is a good start to further improve the *ZT* values when a way to preserve the power factor is accomplished.

4. Conclusions

In summary, p-type $Bi_{0.4}Sb_{1.6}Te_3$ thermoelectric bulk materials were prepared by ball milling the melted ingot with oleic acid and followed by hot pressing. The agglomeration of the nanopowders is alleviated by the introduction of the functional surfactant additive (oleic acid) during ball milling. The growth of the grains during hot pressing is suppressed, which leads to increased phonon scattering for the decreased lattice thermal conductivity. However, power factor was also decreased, leading a *ZT* value of ~1.3 at 373 K, which is about the same as reported before. Higher *ZT* values are expected when a way to preserve the power factor is accomplished.

Acknowledgement: This work is supported by "Solid State Solar-Thermal Energy Conversion Center (S^3TEC)", an Energy Frontier Research Center founded by the U.S. Department of Energy, Office of Science, Office of Basic Energy Science under award number DE-SC0001299 (G. C. and Z. F. R.).

References

[1] B.C. Sales, Smaller is Cooler, Science 295 (2002) 1248.

[2] A. Majumdar, Thermoelectricity in Semiconductor Nanostructures, Science 303 (2004) 777.

[3] R. Venkatasubramanian, E. Siivola, T. Colpitts, B. O'Quinn, Thin-film thermoelectric devices with high room-temperature figures of merit, Nature 413 (2001) 597.

[4] B. Poudel, Q. Hao, Y. Ma, Y.C. Lan, A. Minnich, B. Yu, X. Yan, D.Z. Wang, A. Muto, D. Vashaee, X. Chen, J. Liu, D.S. Dresselhaus, G. Chen, Z.F. Ren, High-Thermoelectric Performance of Nanostructured Bismuth Antimony Telluride Bulk Alloys, Science 320 (2008) 634.

[5] C.M. Jaworski, V. Kulbachinskii, J.P. Heremans, Resonant level formed by tin in Bi_2Te_3 and the enhancement of room-temperature thermoelectric power, Phys. Rev. B 80 (2009) 233201.

[6] J. Shen, T. Zhu, X. Zhao, S. Zhang, S. Yang, Z. Yin, Recrystallization induced *in situ* nanostructures in bulk bismuth antimony tellurides: a simple top down route and improved thermoelectric properties, Energy Environ. Sci. 3 (2010) 1519.

[7] X. Yan, B. Poudel, Y. Ma, W.S. Liu, G. Joshi, H. Wang, Y.C. Lan, D.Z. Wang, G. Chen, Z.F. Ren, Experimental Studies on Anisotropic Thermoelectric Properties and Structures of n-Type $Bi_2Te_{2.7}Se_{0.3}$, Nano Lett. 10 (2010) 3373.

[8] M.S. Dresselhaus, G. Chen, M.Y. Tang, R.G. Yang, H. Lee, D.Z. Wang, Z.F. Ren, J.P. Fleurial, P. Gogna, New Directions for Low-Dimensional Thermoelectric Materials, Adv. Mater. (Weinheim, Ger.) 19 (2007) 1043.

[9] J.R. Szczech, J.M. Higgins, S. Jin, Enhancement of the thermoelectric properties in nanoscale and nanostructured materials, J. Mater. Chem. 21 (2011) 4037.

[10] Y.Q. Cao, X.B. Zhao, T.J. Zhu, X.B. Zhang, J.P. Tu, Syntheses and thermoelectric properties of Bi_2Te_3/Sb_2Te_3 bulk nanocomposites with laminated nanostructure, Appl. Phys. Lett. 92 (2008) 143106.

[11] Y. Ma, Q. Hao, B. Poudel, Y.C. Lan, B. Yu, D.Z. Wang, G. Chen, Z.F. Ren, Enhanced thermoelectric figure-of-merit in p-type nanostructured bismuth antimony tellurium alloys made from elemental chunks, Nano Lett. 8 (2008) 2580.

[12] W. Xie, X. Tang, Y. Yan, Q. Zhang, T.M. Tritt, Unique nanostructures and enhanced thermoelectric performance of melt-spun BiSbTe alloys, Appl. Phys. Lett. 94 (2009) 102111.

[13] N. Gothard, J.E. Spowart, T.M. Tritt, Thermal conductivity reduction in fullerene-enriched p-type bismuth telluride composites, Phys. Status Solidi A 207 (2010) 157.

[14] L.D. Zhao, B.P. Zhang, J.F. Li, M. Zhou, W.S. Liu, J.J. Liu, Thermoelectric and mechanical properties of nano-SiC-dispersed Bi_2Te_3 fabricated by mechanical alloying and spark plasma sintering, J. Alloys Compd. 455 (2008) 259.

[15] T. Zhang, Q. Zhang, J. Jiang, Z. Xiong, J. Chen, Y. Zhang, W. Li, G. Xu, Enhanced thermoelectric performance in p-type BiSbTe bulk alloy with nanoinclusion of ZnAlO, Appl. Phys. Lett. 98 (2011) 022104.

[16] M. Scheele, N. Oeschler, K. Meier, A. Kornowski, C. Klinke, H. Weller, Synthesis and Thermoelectric Characterization of Bi_2Te_3 Nanoparticles, Adv. Funct. Mater. 19 (2009) 3476.

[17] Y.C. Lan, B. Poudel, Y. Ma, D.Z. Wang, M.S. Dresselhaus, G. Chen, Z.F. Ren, Structure Study of Bulk Nanograined Thermoelectric Bismuth Antimony Telluride, Nano Lett. 9 (2009)

1419.

[18] S. Wang, W. Xie, H. Li, X. Tang, High performance n-type $(Bi,Sb)_2(Te,Se)_3$ for low temperature thermoelectric generator, J. Phys. D: Appl. Phys. 43 (2010) 335404.

[19] C. Liao, L.Wu, Enhancement of carrier transport properties of $Bi_xSb_{2-x}Te_3$ compounds by electrical sintering process, Appl. Phys. Lett. 95 (2009) 052112.

[20] W.S. Liu, Q.Y. Zhang, Y.C. Lan, S. Chen, X. Yan, Q. Zhang, H. Wang, D.Z. Wang, G. Chen, Z.F. Ren, Thermoelectric Property Studies on Cu-Doped n-type $Cu_xBi_2Te_{2.7}Se_{0.3}$ Nanocomposites, Adv. Energy. Mater. 1 (2011) 577.

Figure Captions

Figure 1. XRD patterns of the as-prepared bulk $Bi_{0.4}Sb_{1.6}Te_3/x$ with different concentrations of OA (x = 0, 0.5, 1.0, 1.5, 2.0, and 2.5 wt.%).

Figure 2. SEM images of the ball-milled $Bi_{0.4}Sb_{1.6}Te_3$ powder without additive OA (a) and with 2.0 wt.% additive OA (d). TEM images of the ball-milled $Bi_{0.4}Sb_{1.6}Te_3$ powder without additive OA (b) and with 2.0 wt.% additive OA (e). HRTEM images of the ball-milled $Bi_{0.4}Sb_{1.6}Te_3$ powder without additive OA (c) and with 2.0 wt.% additive OA (f).

Figure 3. SEM images of the as-prepared bulk samples $Bi_{0.4}Sb_{1.6}Te_3/x$ with different concentrations of additive OA x = 0, 0.5, 1.0, 1.5, 2.0, and 2.5 wt.% for (a), (b), (c), (d), (e), and (f), respectively.

Figure 4. Temperature dependence of the electrical conductivity (a), Seebeck coefficient (b), total thermal conductivity (c), lattice thermal conductivity (d), power factor (e), ZT (f), thermal diffusivity (g) and specific heat (h) of the as-prepared $Bi_{0.4}Sb_{1.6}Te_3/x$ with different concentrations of OA (x = 0, 0.5, 1.0, 1.5, 2.0, and 2.5 wt.%).

TABLE I. Volumetric density, carrier concentration, and Hall mobility at room temperature of the as-prepared $Bi_{0.4}Sb_{1.6}Te_3/x$ with x = 0, 0.5, 1.0, 1.5, 2.0, and 2.5 wt.% .

$Bi_{0.4}Sb_{1.6}Te_3/x$ (x in wt.% per formula weight)	x = 0	x = 0.5	x = 1.0	x = 1.5	x = 2.0	x = 2.5
Volumetric density (gcm^{-3})	6.65	6.40	6.00	5.92	6.01	5.90
Carr. Conc. ($\times 10^{19}, cm^{-3}$)	4.29	4.27	2.94	2.96	3.09	3.22
Hall Mobility ($cm^2V^{-1}s^{-1}$)	163	162	179	172	179	147

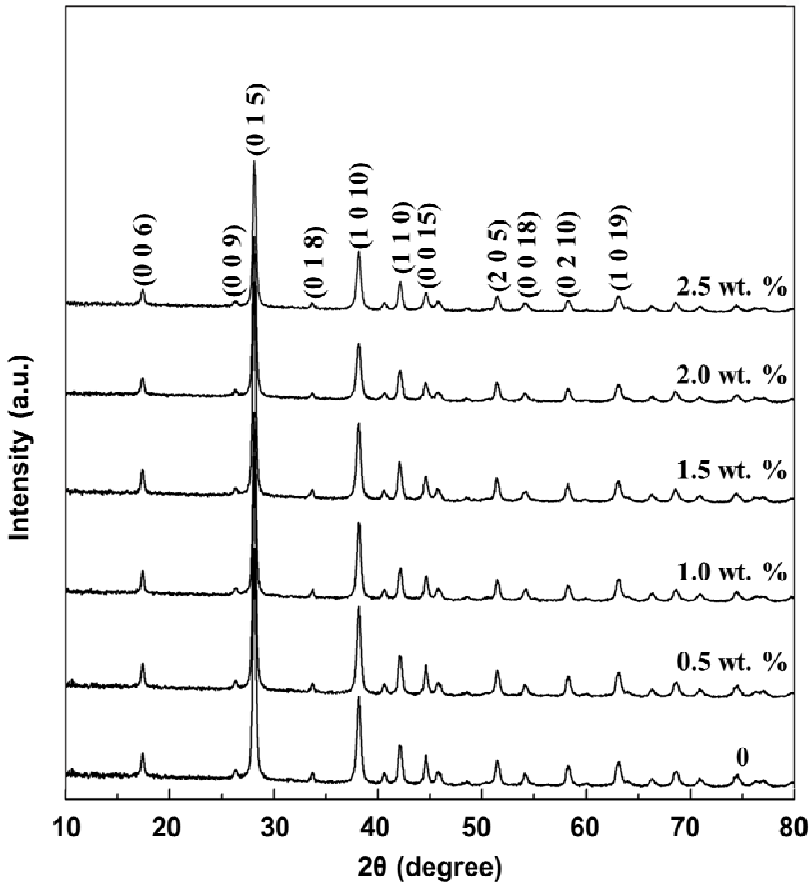

Figure 1 Qian Zhang *et al.*

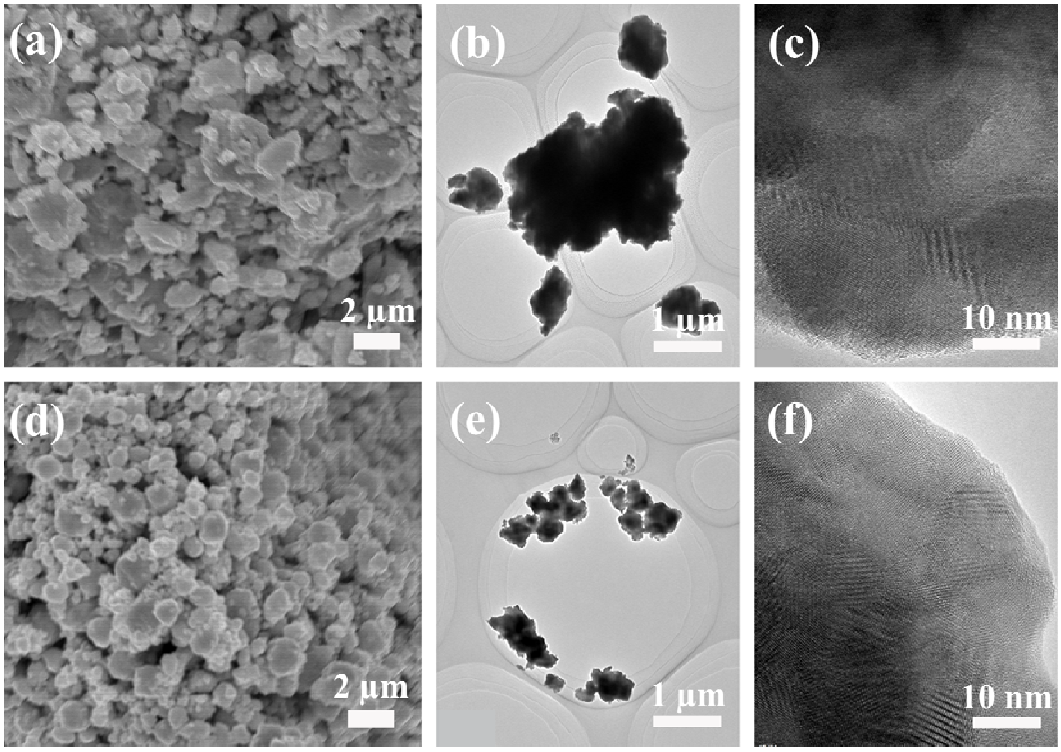

Figure 2 Qian Zhang *et al.*

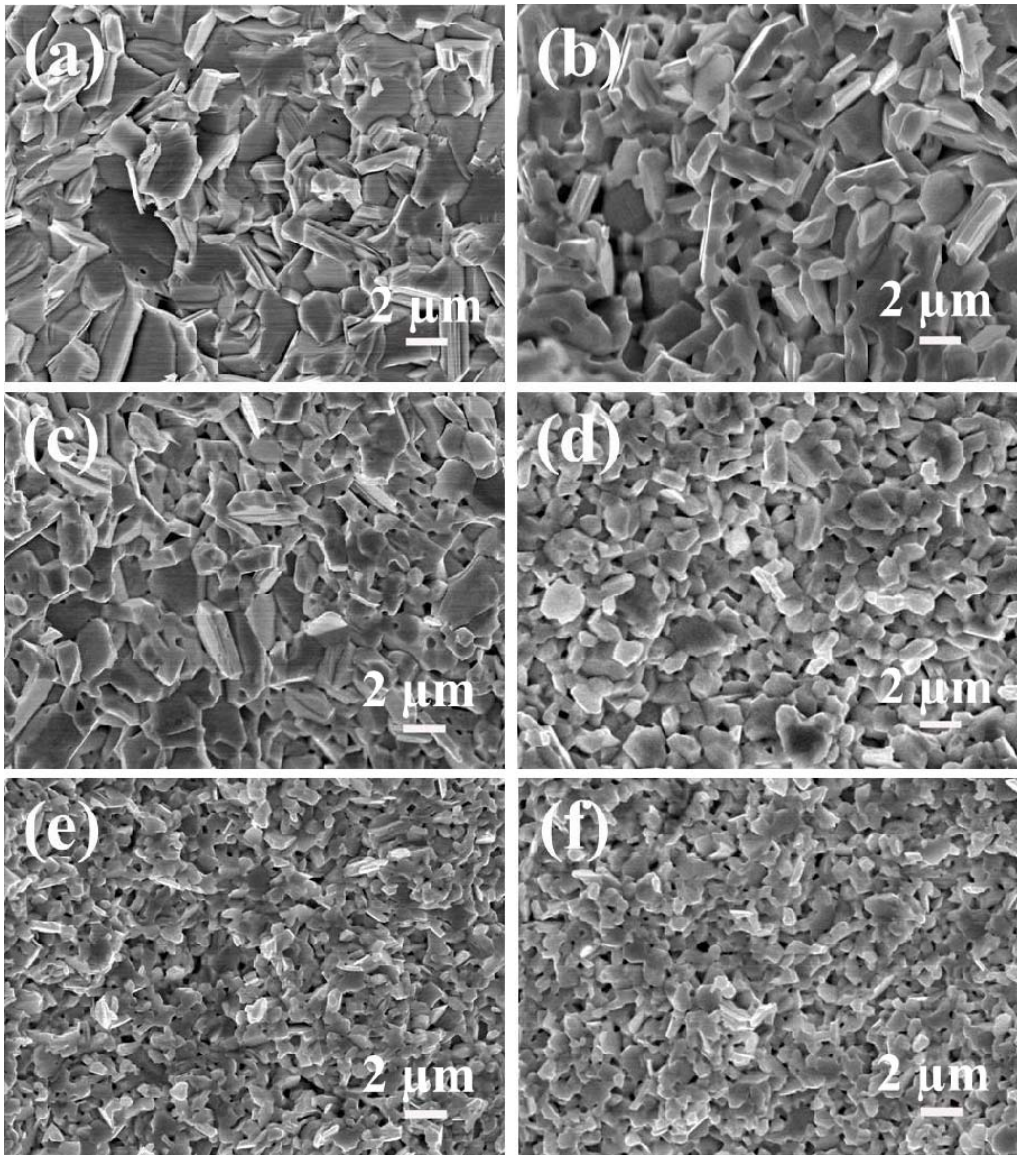

Figure 3 Qian Zhang *et al.*

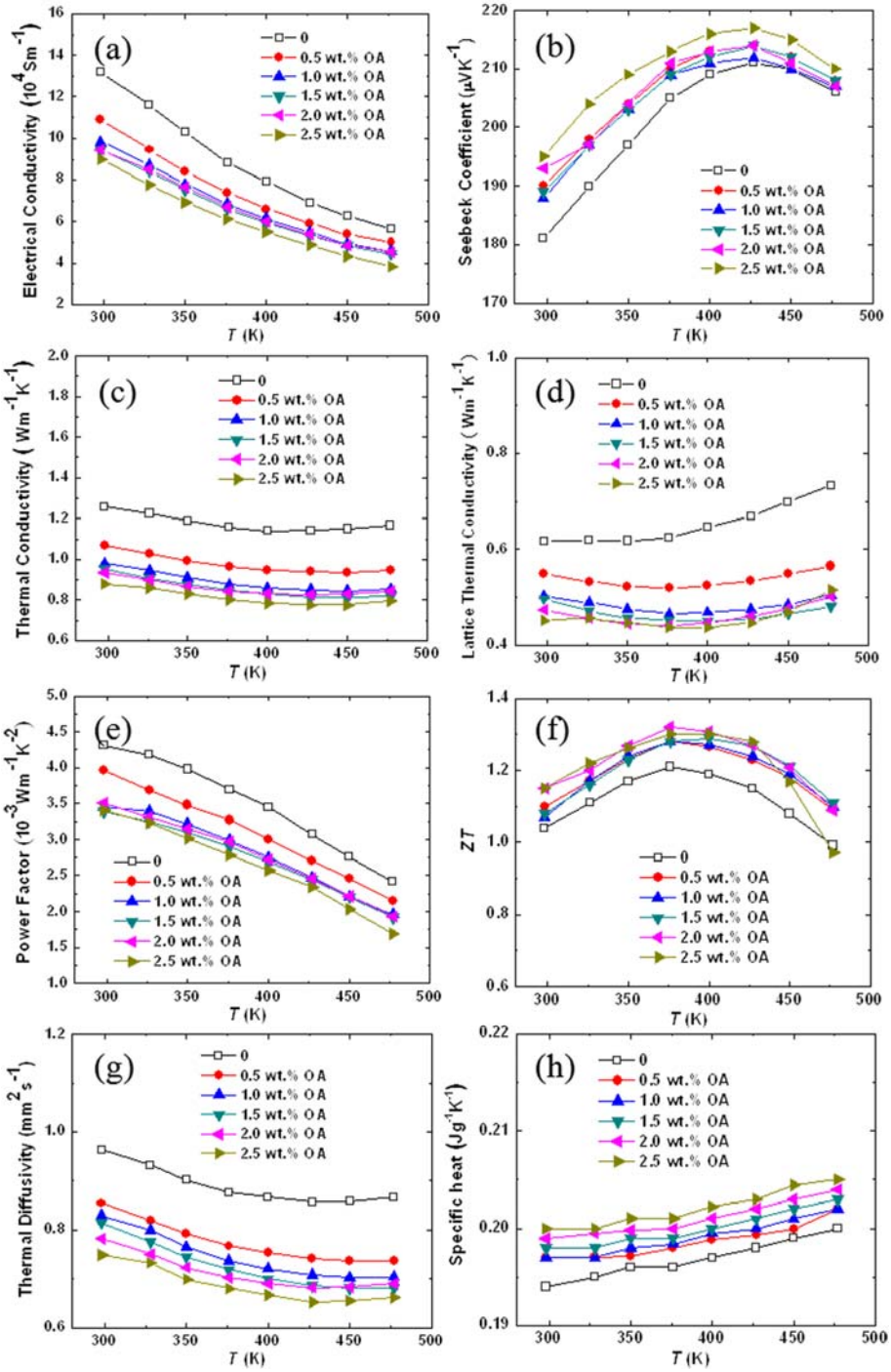

Figure 4 Qian Zhang *et al.*